The Thesis Committee for Sorin S Secara
Certifies that this is the approved version of the following thesis:

Liquefaction-Induced Lateral Displacements from the Canterbury Earthquake Sequence in New Zealand Measured from Remote Sensing Techniques

APPROVED BY
SUPERVISING COMMITTEE:

Supervisor:

Ellen Rathje

Brady Cox

Liquefaction-Induced Lateral Displacements from the Canterbury Earthquake Sequence in New Zealand Measured from Remote Sensing Techniques

by

Sorin S Secara, B.C.E.

Thesis

Presented to the Faculty of the Graduate School of

The University of Texas at Austin

in Partial Fulfillment

of the Requirements

for the Degree of

Master of Science in Engineering

The University of Texas at Austin

May 2016

Acknowledgements

I would like to thank Dr. Ellen Rathje for her support and guidance during the entire time that she has been my advisor. I am incredibly grateful for her all the patience, dedication and kindness and her expertise and insight have proven invaluable. It has been an honor for me to have such a wonderful and intelligent mentor. I also want to thank Dr. Brady Cox for all that he has taught me, his support and time.

I would like to thank my girlfriend Hallie, my best friend Ian and my family for their support throughout my time at the University of Texas. Your encouragement and love have kept me focused and carried me through this entire process.

I would also like to thank the other professors at the University of Texas who have invested in my professional and personal development. I feel blessed to have been able to attend such a prestigious university. I also want to thank the entire Geotechnical Department and its body of graduate students who have been both partners and friends in my endeavors at UT.

Abstract

Liquefaction-Induced Lateral Displacements from the Canterbury Earthquake Sequence in New Zealand Measured from Remote Sensing Techniques

Sorin S Secara, M.S.E.

The University of Texas at Austin, 2016

Supervisor: Ellen Rathje

Liquefaction is a significant earthquake hazard that can generate large horizontal displacements associated with lateral spreading and these displacements cause considerable damage. To improve our understanding of liquefaction-induced lateral spreading and the models that can be used to predict the associated displacements, the collection of high quality field data on lateral spreading displacements is essential. Remote sensing techniques, in particular optical image correlation using satellite imagery, can be used for this purpose. This thesis investigates optical image correlation of satellite images as a remote sensing technique for this purpose using images from the 2010-2011 Canterbury earthquake sequence in New Zealand.

Optical image correlation uses two optical images – one before and one after the investigated event – to measure displacements that have occurred between the time of the two image acquisitions. The correlation analysis calculates the horizontal displacement at

a specified spacing, and the displacements are post-processed and filtered to attain the final displacement field.

The displacement results from optical image correlation agreed favorably with qualitative field observations of the severity of liquefaction and lateral spreading, as well as the general crack patterns along the Avon River. A more quantitative comparison was performed using field measured displacements along four linear transects that extended perpendicular from the Avon River. The displacements from optical image correlation also agreed favorably with the field measured displacement profiles, although the optical image correlation displacements somewhat larger than the field measurements. This discrepancy occurs because field measurements are based on discrete measurements of crack width, while the optical image correlation are based on average displacements over larger areas and include displacements associated with ductile movements that may not result in cracking.

The results from this research show that optical image correlation of satellite imagery pairs can provide accurate and detailed measurements of horizontal displacements due to liquefaction and lateral spreading. This approach can be used to create more complete and detailed databases of liquefaction-induced movements, which can be used to improve current predictive models for lateral spread displacements. Future post-earthquake investigations and research should make use of optical image correlation to document the displacements associated with liquefaction.

Table of Contents

List of Tables

List of Figures

1. Introduction

Liquefaction is a phenomenon that occurs when loose, saturated sandy soils are subjected to a rapid loading such as earthquake shaking, and the resulting pore pressure generation leads to a sudden reduction in the strength and stiffness of the soil. The consequences of liquefaction are significant and include sand boils, slope failures, foundation failures, excessive settlement, and lateral spreading. Horizontal displacements due to liquefaction-induced lateral spreading is one of the main causes of liquefaction damage to infrastructure because of the development of ground cracks that can simply pull a structure apart. Despite the fact that lateral spread displacements cause significant infrastructure damage, our ability to predict these displacements is imperfect and imprecise due to the limited field data that exist regarding liquefaction-induced horizontal movements.

The traditional method of measuring horizontal displacements due to lateral spreading is to manually measure the widths of the cracks associated with lateral spreading. These cracks generally run perpendicular to the direction of movement and are measured using either a measuring tape or GPS points on both edges of the cracks. Unfortunately, this method suffers from some drawbacks. First, it is assumed that all lateral spread displacement is manifested in cracks and that the material between the cracks acts as a rigid block. Additionally, the field measurement of crack widths can be inaccurate due to the presence of ejecta or sloughing of crack edges, accessibility issues may prohibit some measurements, and the measurement process can be very time consuming.

Remote sensing techniques, such as optical image correlation of satellite imagery (Leprince et al. 2007), can mitigate the challenges associated with field measurement of lateral spread displacements. A satellite imagery correlation analysis covers a large area

(e.g., over 30 km2), can be done in matter of days by a single person, and the satellite imagery is inexpensive, even for high resolution (i.e., 0.5 m) images. These images can be obtained for an entire region, thus eliminating accessibility issues, and they also measure the overall horizontal movement due to lateral spreading, not only the visible surface cracks. Using optical image correlation instead of traditional field measurement techniques can improve and expand the existing databases of lateral spreading displacements, which in turn will allow for the development of more reliable models to predict lateral spread displacements.

This paper applies the optical image correlation technique to the 2010-2011 Canterbury Earthquake Sequence in New Zealand. This earthquake sequence includes the M 7.1 Darfield earthquake on September 4th 2010, the M 6.3 Christchurch earthquake on February 22nd 2011, the M 6.3 earthquake on June 13th 2011, and the M 6.0 earthquake on December 23rd 2011. The Christchurch earthquake was the most devastating of the four earthquakes, severely damaging infrastructure, inducing significant liquefaction, and claiming 185 lives (Cubrinovski et al. 2011). The Darfield earthquake also caused significant damage (Green et al. 2010). Figure 1 shows the ground surface observations of liquefaction for both the Darfield and Christchurch earthquakes in an area along the Avon River, east of the Christchurch Central Business District. These data show moderate to severe lateral spreading along much of the Avon River, with the extent of lateral spreading larger for the Christchurch event.

Although Figure 1 shows valuable information about the liquefaction effects in Christchurch, the observations are qualitative rather than quantitative. In this paper quantitative measurements of lateral spread displacements for the Christchurch earthquake and the full Canterbury earthquake sequence will be derived from optical image correlation. The optical image correlation technique will be introduced, and the details of

the data processing chain will be discussed. The displacements measured from optical image correlation will be compared with other sources of data, both quantitative and qualitative, regarding the liquefaction effects in Christchurch.

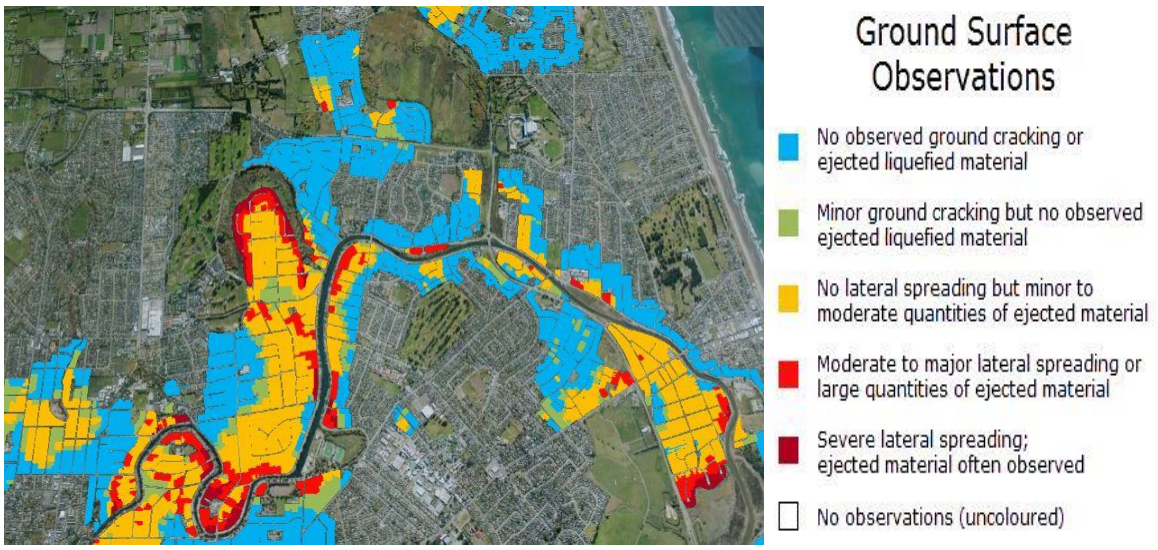

(a)

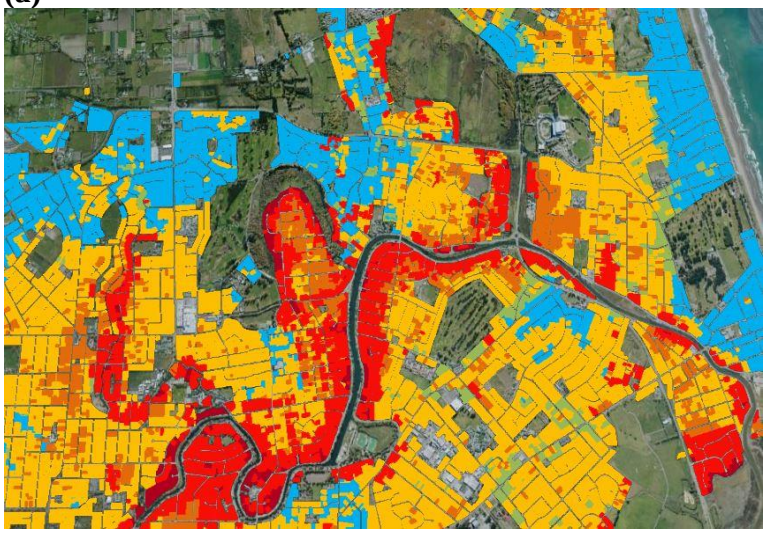

(b)

Figure 1: (a) Observed liquefaction from the Darfield earthquake (b) Observed liquefaction from the Christchurch earthquake (Canterbury Geotechnical Database 2013)

2. Optical Image Correlation Analysis

Optical image correlation uses two optical images – one before and one after the event or series of events under investigation – and measures displacements that have occurred during the time frame between the two image acquisitions. The two images are selected based on their overlapping coverage of the area of interest, the quality of the images, and the similarity in the acquisition geometry for the images. The images are then aligned as precisely as possible using orthorectification (i.e. corrections for topography) and co-registration. Common tie points between the two images are used to co-register the two images, which involves warping the post-event image onto the pre-event image. Finally, the correlation analysis is used to calculate the horizontal displacement at a specified spacing, and the displacements are post-processed and filtered to attain the final displacement field.

2.1. Image Selection and Pre-Processing

The first step in optical image correlation involves the selection of a suitable image pair and the pre-processing of the two images. Image selection is a critical part of the process because it directly impacts the accuracy of the resulting displacements. The extent of the area of interest is established first and each of the two images should cover an area larger than this extent because the co-registration process will affect the edges of the warped image. The images initially do not need to be the same size because they can be cropped during pre-processing. Because weather conditions during acquisition of the images can affect their quality, it is best to search for image pairs that have the least amount of cloud coverage.

After identification of candidate pre-event and post-event images based on coverage and image quality, the acquisition geometry parameters of the images are considered. These parameters describe the orientation of the satellite sensor during acquisition (Figure 2) using the azimuth angle (α) and the off-nadir angle (β). The azimuth angle is the angle measured clockwise from north while the off-nadir angle is the angle between the vertical and the direction of the sensor. When selecting an image pair these angles should be as similar as possible so as to minimize false displacements due to DEM errors (Scherler et al. 2008). Additionally, the off-nadir angle should be as small as possible to minimize image distortions due to topography, and it is preferable that the two images be taken during a similar time of year so they are similarly affected by sun illumination. Additional information about these issues can be found in Martin (2014).

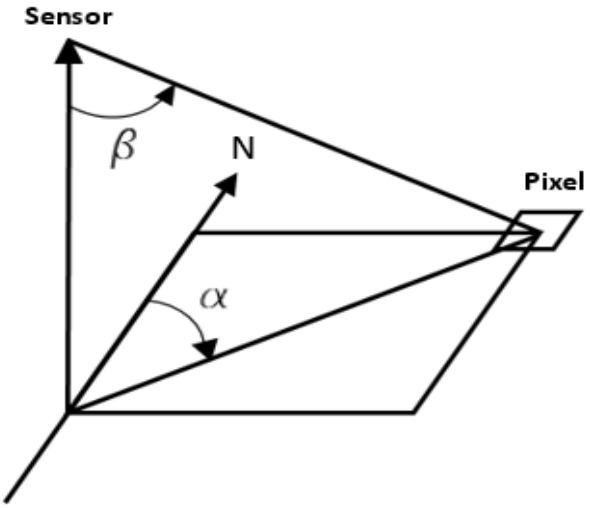

Figure 2: Image acquisition parameters: Off-nadir angle (β) and Azimuth angle (α)

After the image pair is selected, pre-processing involves orthorectification and co-registration. Orthorectification corrects for topographic effects (i.e., parallax) on the

ground surface when images are obtained at off-nadir angles greater than zero (i.e., non-vertical). Distortions are more significant for more variable topography and larger off-nadir angles. Orthorectification is done using a digital elevation model (DEM) that accounts for the elevation of each pixel and corrects for the effects of parallax and scaling. Orthorectification not only leads to a more accurate visual representation of each image individually, but also allows for better matching between pixel patterns in the two images, which is important to identify higher quality tie points. After both images are orthorectified, they are cropped using the same clipping shapefile representing the area of interest. The open source software GDAL (Geospatial Data Abstraction Library, GDAL 2012) and a 90 m resolution DEM from the Shuttle Radar Topography Mission (SRTM, USGS 2004) were used for the orthorectification process.

Co-registration aligns the two images very accurately based on identifying the same objects/features (i.e., tie points) in both images. This process also removes any distortions remaining after the orthorectification or due to initial geo-referencing misalignment. For high quality co-registration, the set of tie points should be both reliable and well distributed across the area of interest. The computer program ENVI (Exelis Visual Information Solutions 2013) and its automatic registration function are used to identify tie points in the two images. The ENVI automatic registration function uses two windows to identify tie points: a moving window and a search window. The moving window is a patch of pixels defined in the first image and the analysis scans the second image looking for a matching pixel pattern, as computed by the correlation coefficient. The location in the second image with the largest correlation coefficient is identified as a candidate tie point. The search window is a subset of the larger image within which the moving window shifts until it identifies a tie point. Thus, the search window size must be greater than the moving window size. After ENVI finds candidate tie points across the image, points are rejected that have

a correlation coefficient smaller than the minimum specified by the user (typically specified as 0.7). ENVI extracts a final set of tie points from the remaining candidate tie points based on the area chip size. The area chip size is a constant sized pixel area and ENVI identifies one or two tie points per area chip.

ENVI allows the user to input the desired number of candidate tie points, the moving window size, the search window size, the area chip size, and the minimum correlation coefficient. As noted earlier, the search window size must be larger than the moving window size. For both the search window and the moving window, increasing size leads to more reliable tie points but also longer processing times. The maximum number of tie points that can be requested is obtained by dividing the total pixel area of the image by the moving window size, which means that a larger moving window limits the number of candidate tie points. The area chip size should always be larger than the moving window size, and preferably larger than the search window size, so that the final set of tie points only includes the best candidate tie points.

The final set of tie points obtained by ENVI is used in an initial co-registration, which involves warping one image to the other using a first-order polynomial. A value for the root mean square error (RMSE) for the warping polynomial is calculated, which represents the scatter of the tie points about the best fit polynomial. The final processing of tie points is performed using a Python script developed by Martin (2014). Here, tie points are removed that are located within areas that are expected to have moved (e.g., along rivers for lateral spreading, within landslides) or are within areas where the tie points likely are unreliable (e.g., water bodies, cloud cover, highly monotone areas). Tie points with correlation coefficients less than 0.95 are also removed. Finally, tie points with large errors relative to the warping polynomial are systematically eliminated until a desired RMSE value is reached. Tie points with large residuals are removed because large residuals

potentially indicate false-positive tie points (i.e., the areas identified in the two images are not the same).

2.2 CORRELATION ANALYSIS AND POST-PROCESSING

The correlation analysis is performed using an extension feature in ENVI called COSI-Corr (Leprince et al. 2007). The procedure is fairly similar to the one used to find the tie points for the pre-processing step; it involves a methodical search of matching pixel patterns for a patch of pixels in the two images. The pre-event image is divided into smaller pixel areas called a chip window. The software uses each pre-event chip window, as shown by the green rectangle in Figure 4a, and compares it with a multitude of post-event chip windows both in its original coordinate location (orange rectangle, Figure 4b) and surrounding locations (red rectangles, Figure 4b). COSI-Corr performs the correlation analysis for each post-event chip window and identifies the best possible match, as indicated by the green rectangle in Figure 4b. The distance between the locations of the matched windows in the two images represents the horizontal displacement. Using the results from the correlation analysis, COSI-Corr computes a signal-to-noise-ration (SNR) for the matched window, with an SNR of 0 representing no correlation and an SNR of 1 representing perfect correlation. The same correlation analysis and displacement analysis is performed for large suite of chip windows in the pre-event image, with each new chip window located a user-specified number of pixels from the previous chip window.

Figure 3: Optical Image Correlation Process. (a) Pre-event image. The green box represents the chip window to be matched. (b) Post-event image. The orange box represents the initial location of the pre-event chip window in the post-event image, the red boxes represent a sub-set of locations assessed for match, and the green box represents the matching chip window.

The COSI-Corr analysis provides a set of initial displacement results, separated into north-south and east-west displacements, each of which has an associated SNR. A Python script is used to remove displacements for which the value of SNR is less than a specified threshold. This threshold typically is specified as 0.95.

2.3. APPLICATION OF OPTICAL IMAGE CORRELATION TO CHRISTCHURCH, NEW ZEALAND

Optical image correlation was applied to images from Christchurch, New Zealand to investigate displacements due to liquefaction-induced lateral spreading during the 2010-2011 Canterbury earthquake sequence. One image pair was identified to investigate the displacements during the 2011 Christchurch earthquake and another pair was selected that

spans the entire earthquake sequence (Table 1). This second pairs allows provides measurements of the cumulative displacements from the four earthquake events. For both image pairs, note that the azimuth and off-nadir angles are within a few degrees of each other.

Table 1. Acquisition geometry parameters for image pairs used to analyze the Christchurch earthquake and Canterbury earthquake sequence

Event	**Date**	**Azimuth** (degrees)	**Off-Nadir** (degrees)
Christchurch earthquake	September 21, 2010	55.1	19.8
	February 26, 2011	51.1	18.2
Canterbury earthquake sequence	January 7, 2010	110.5	17.2
	January 3, 2013	110.2	18.1

Orthorectification and co-registration of the two sets of image pairs were performed using the procedures outlined previously and a 250 m wide buffer around the Avon River within which no tie points were allowed (Figure 4). For the Christchurch earthquake image pair (Figure 5a), 10,000 tie points were requested with a search window size of 111 square pixels, a moving window size of 81 square pixels, an area chip size of 128 square pixels, and a minimum correlation coefficient of 0.7. This analysis yielded 3,967 initial tie points which were then filtered using the river buffer and removing tie points until an RMSE of 0.30 m was achieved. This resulted in 1,686 reliable tie points (~47 tie points/km2) for use in the co-registration. For the Canterbury earthquake sequence (Figure 5b), 10,000 tie points were requested using the same window sizes and parameters for the Christchurch earthquake images. This analysis yielded 4,135 initial tie points which were then filtered

using the river buffer and removing tie points until an RMSE of 0.325 m was achieved. This resulted in 1,863 tie points (~ 44 points/km2) for use in the co-registration. The sizes of the search window and moving window were selected based on sensitivity studies in which the number and distribution of the tie points and quality of the co-registration was evaluated for a range of window sizes. This sensitivity analysis is required when analyzing any new image pair.

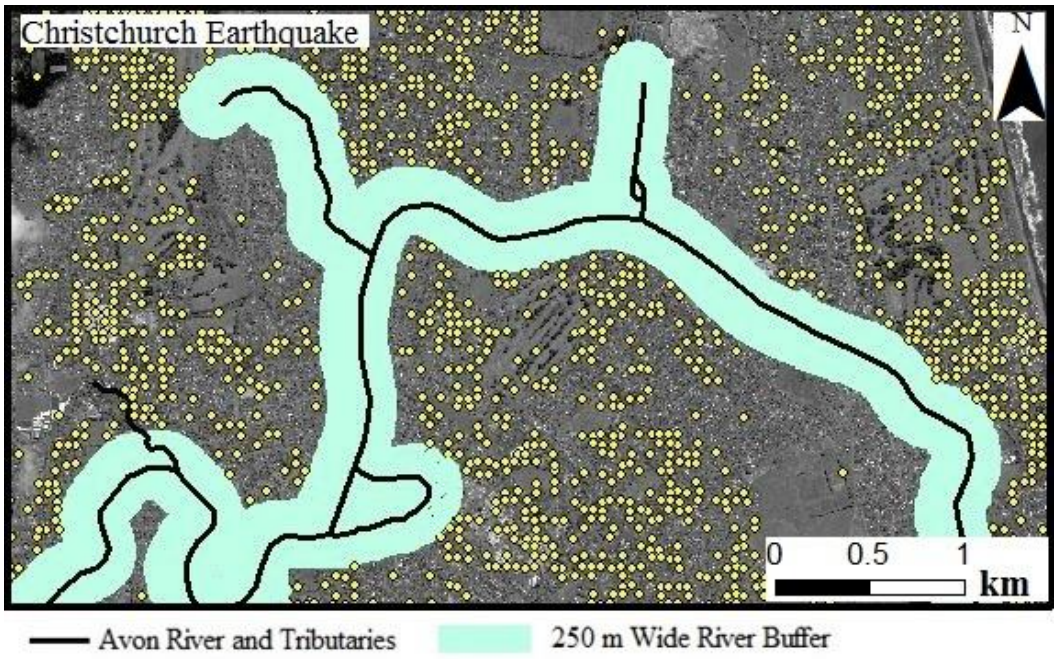

(a)

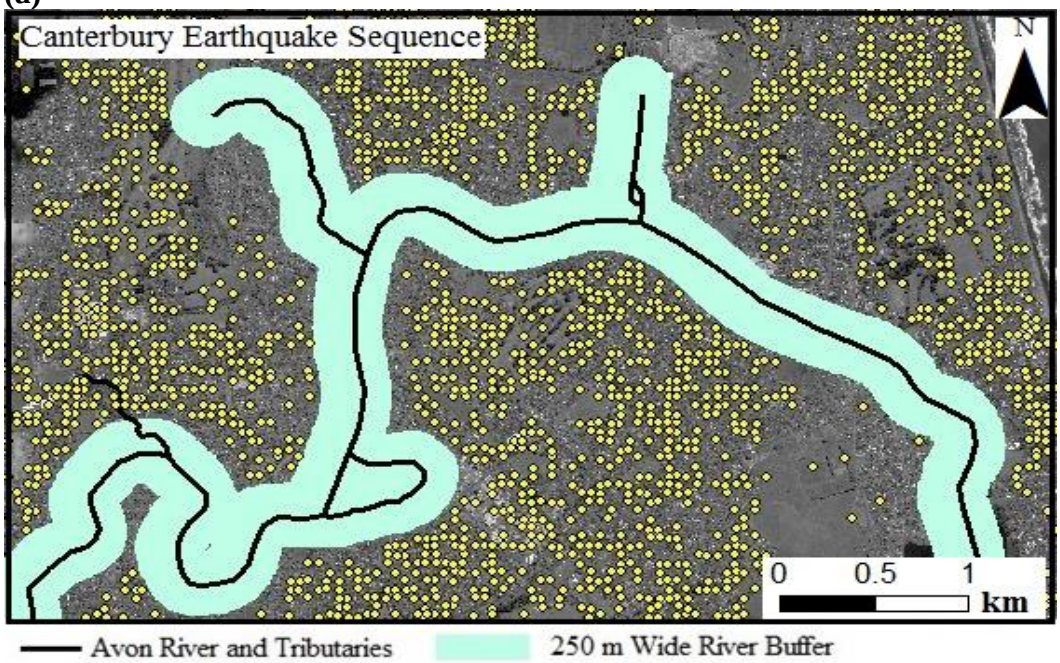

(b)

Figure 4: Tie points used in co-registration of the (a) Christchurch earthquake image pair and (b) Canterbury earthquake sequence image pair

Correlation analysis was performed on the two sets of images using the program COSI-Corr (Leprince et al. 2007). For each analysis a chip window of 128 by 128 pixels (64 m) was used with a step size of 32 pixels, which produced a displacement measurement every 16 m. This chip window size was selected after investigating other sizes and qualitatively evaluating the results. Results with an SNR less than 0.95 were removed.

Based on a number of factors (e.g. image pixel resolution, tie point quality) the precision of the displacement results can vary. To asses this precision histograms of the displacements in the non-moving areas can be used (Debella-Gilo and Kääb 2012). Figure 5 shows the histograms of north-south (NS) and east-west (EW) displacements in the non-moving areas for the results from the Christchurch earthquake image pair and the image pair for the Canterbury earthquake sequence. For all of the cases shown, the means are close to zero (i.e., less than 0.05 m) and standard deviations are less than 0.25 m (Table 2). The square root of the sum of squares of the EW and NS standard deviations is close to 0.30 m for the two sets of analyses. This value of 0.3 m is considered the smallest resolvable displacement by the optical image correlation results presented here.

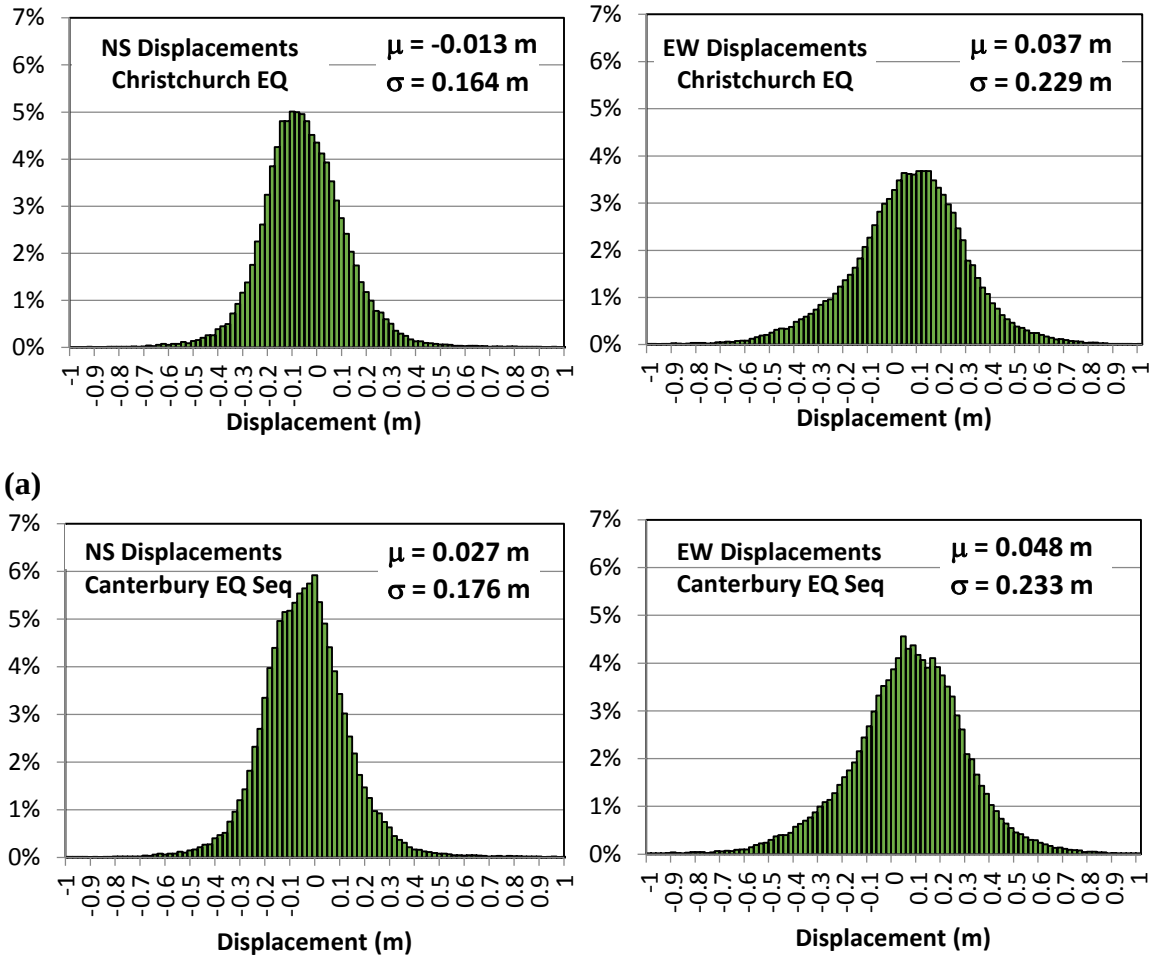

Figure 5: Displacement histograms in non-moving areas (a) Christchurch earthquake image pair and (b) Canterbury earthquake sequence image pair

Table 2. Mean and standard deviation values for displacement results from the Christchurch earthquake and Canterbury earthquake sequence in non-moving areas

		Mean (m)	Standard Deviation (m)
Christchurch Earthquake	**NS**	-0.013	0.164
	EW	0.037	0.229
Canterbury earthquake sequence	**NS**	0.027	0.176
	EW	0.048	0.233

3. Liquefaction induced displacements from optical image correlation

3.1. CHRISTCHURCH EARTHQUAKE

Using the methodology described in Section 2, the horizontal displacements induced by the 2011 Christchurch earthquake were computed using the program COSI-Corr (Leprince et al. 2007). Figure 6 shows the computed displacements, with the NS displacements and the EW displacements plotted separately. Displacements are only shown for locations with SNR greater than 0.95. Additionally, displacements less than the precision threshold of 0.3 m are shown as 0 m for better visualization of the lateral spread zones. The largest displacements are concentrated along the Avon River and other creeks in its vicinity. In areas where the river flows predominantly EW the displacements are primarily NS, and conversely where the river flows predominantly NS the displacements are predominantly EW. Thus, the displacements are consistent with spreading towards the river. In most areas the displacements are concentrated within about 200 m to 300 m of the river, but displacements extend more than 1 km north from the river in some areas in the eastern part of the study area.

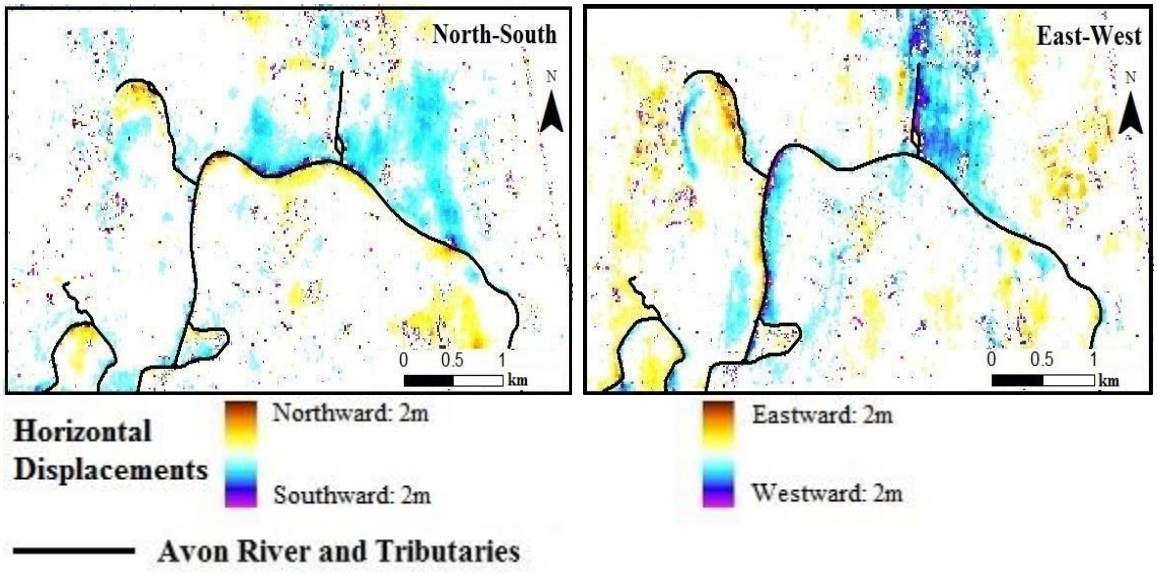

Figure 6: Horizontal displacement results from optical image correlation for the Christchurch earthquake

To assess the displacement results from optical image correlation for the Christchurch event, the displacements are compared with both mapped cracking patterns and observed liquefaction effects from field reconnaissance (Figure 7). For this comparison the displacement amplitudes are used, which are computed as the square root of the sum of squares of NS and EW displacements. The displacement amplitudes are shown in Figure 7a for the southwestern part of the study area, along with the observed liquefaction-induced ground cracks with widths greater than 50 mm. As expected, the computed displacements are largest near the river and their magnitude decreases with distance from the river. The cracking patterns are parallel to the river, their locations are consistent with the computed displacements, and they generally bound the largest displacements (~ 0.5 m and larger). Figure 7b shows the qualitative observations of liquefaction effects across the same southwestern part of the study area. Again, there is general agreement between the

observed displacements in Figure 7a and the areas identified as having experienced moderate/major and severe lateral spreading in Figure 7b.

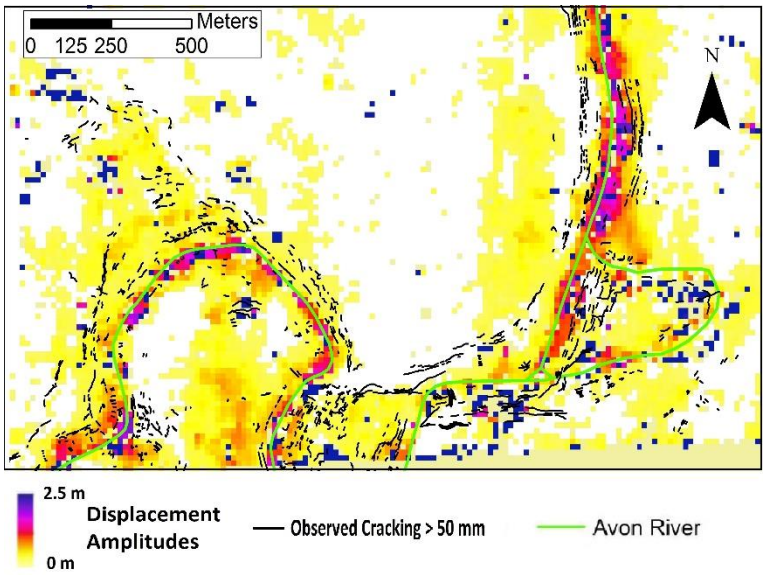

(a)

(b)

Figure 7: (a) Displacement amplitudes from optical image correlation and field measured ground cracking for the Christchurch earthquake and (b) ground surface observations of liquefaction effects for the Christchurch earthquake (Canterbury Geotechnical Database 2013)

3.2 CANTERBURY EARTHQUAKE SEQUENCE

The cumulative horizontal displacements across the four earthquakes from the Canterbury earthquake sequence were computed using optical image correlation and the image pair that spanned the full earthquake sequence (Table 2). Figure 8 shows the computed NS and EW displacements across a study area slightly larger than previously shown for the Christchurch earthquake. Displacements were computed across a larger extent simply due to the larger extent of the common parts of the image pair.

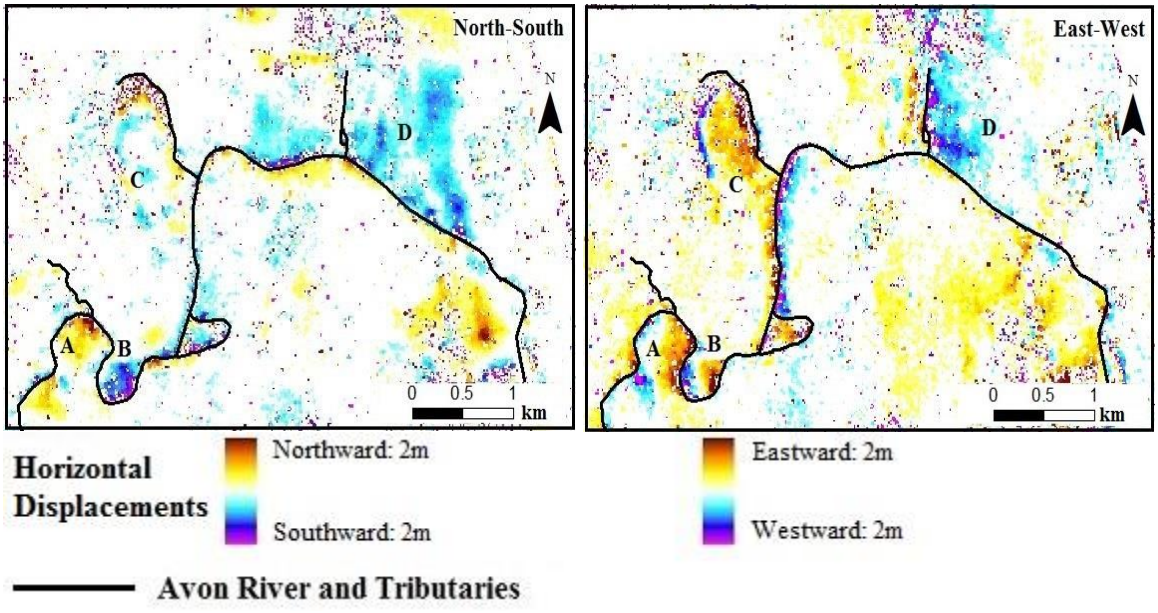

Figure 8: Horizontal displacements measured by optical image correlation for the Canterbury earthquake sequence

The displacement patterns for the Canterbury earthquake sequence (Figure 8) are very similar to those for the Christchurch earthquake (Figure 6), although the displacement amplitudes for the Canterbury earthquake sequence are larger overall given that they include displacements from multiple earthquakes, including the 2010 Darfield earthquake. For example, areas A and B show significantly larger displacements in both the NS and

EW directions compared to the Christchurch event, while area D only shows moderately larger displacements. It should be noted that area B is near the edge of the image for the Christchurch earthquake image pair and thus the displacements in that area for the Christchurch earthquake were likely influenced by edge effects. Area C displays similar displacements in the NS direction, but larger displacements across the full earthquake sequence for the EW direction.

4. Comparison of displacements from different data sources

Other remote sensing techniques, as well as field reconnaissance, can be used to measure horizontal displacements due to lateral spreading. These alternative techniques provide a quantitative mechanism to evaluate the displacements measured by optical image correlation. To assess the results from the optical image correlation analysis, displacements from both LIDAR point clouds and correlation analysis using air photos are used.

Horizontal displacement measurements from LIDAR use point clouds from before and after the February 2011 Christchurch earthquake in a sub-pixel correlation analysis (Beavan et al. 2012a). This analysis is similar to the optical image correlation technique previously described, except that the elevation of each point in the point cloud was used in the correlation analysis. Because the LIDAR point clouds use an absolute reference frame, the displacements due to the fault rupture must be removed from the displacements to obtain local displacement from liquefaction alone. Models of horizontal tectonic movements from GNS Science dislocation models were used for this purpose (Beavan et al. 2012b). Also, the LIDAR analysis only provides displacements in areas with distinct topographic features, such as buildings, and thus areas without these features, such as parks, fields, and roadways along the river, do not have any displacements reported. The results from the LIDAR analysis provided displacements ever 8 m and were smoothed with a non-local means filter (Beavan et al. 2012a).

For the air photo analysis, pre and post-event air photos were supplied by Christchurch City Council and have a pixel resolution of 0.125 m as compared with the 0.5 m pixel size for the satellite images. The analysis process for the air photos is the same as for the satellite images with a few differences due to particularities of each acquisition method (e.g. image resolution, artefacts created by path flight lines) which in turn change

optimal parameters to be used in the analysis. The requested number of initial tie points was 25,000, with a search window size of 331 square pixels, a moving window size of 245 square pixels, and a chip size of 256 square pixels. These parameters yielded 7,865 initial tie points which were then filtered using the river buffer and removing tie points until an RMSE of 0.325 m was achieved. This resulted in 1,686 reliable tie points for use in the co-registration. Displacements were computed using COSI-Corr, a chip window of 128 by 128 pixels, and a step size of 32 pixels, which produced a displacement measured every 8 m.

Figure 9 shows the NS and EW horizontal displacements for the Christchurch earthquake derived from optical image correlation of satellite imagery, correlation analysis of LIDAR point clouds, and optical image correlation of air photos. The displacement patterns from the satellite imagery and LIDAR generally are consistent, with similar zones of large displacement identified. The LIDAR results appear smoother due to the non-local means filter that was applied (Beavan et al. 2012a).

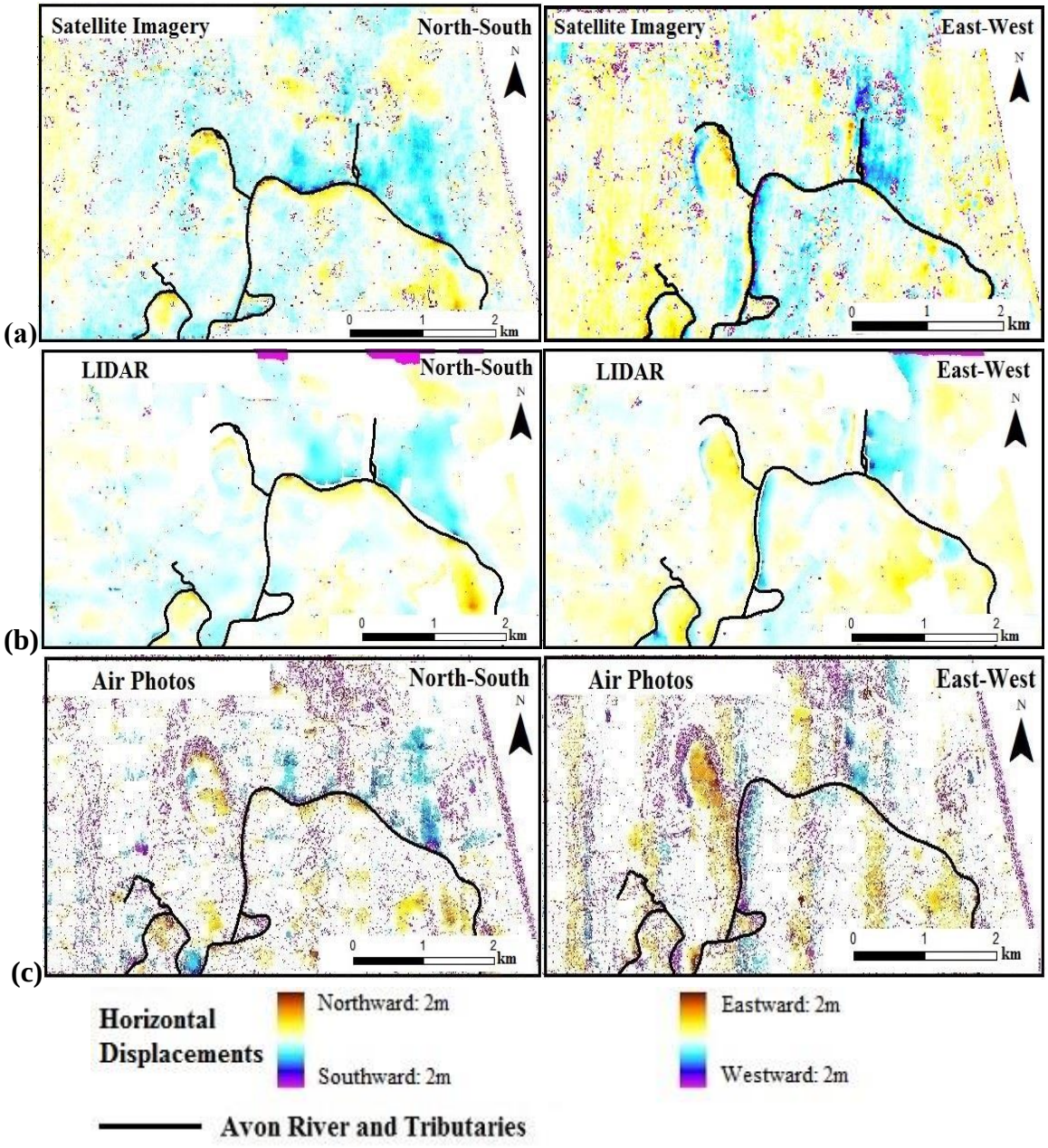

Figure 9: Horizontal displacements for the Christchurch earthquake from different remote sensing techniques (a) optical image correlation of satellite images (b) correlation analysis of LiDAR- point clouds (Beavan et al. 2012a), and (c) optical image correlation of air photos.

Considering the displacements from the analysis of air photos (Figure 9c), one important difference is the high level of noise present as compared with the other two analyses. The very high resolution for these images leads to more false positives during the correlation process, which ultimately leads to erroneous estimates of displacement. Also, fewer displacement measurements met the specified minimum SNR of 0.95 and were discarded. Some of the problems with the air photo analysis are due to errors in the stitching together of the image strips which form the final image and the fact that the metadata from the image acquisitions were not available. Nonetheless, some of the significant displacement patterns can be distinguished in the air photo results, most noticeably the EW displacements in the oxbow lake to the northwest of the Avon River.

A more detailed and quantitative assessment of the displacement measurements from remote sensing can be achieved using ground survey measurements of crack widths along transects. These ground survey displacement measurements are developed by summing the cumulative displacements of the crack widths along a transect. Robinson et al. (2012) measured displacements after the Darfield and Christchurch earthquakes along more than 100 transects, and a few of these transects were used to compare with the remote sensing displacements from optical image correlation and LIDAR. Given the transect locations, displacement profiles along these lines from the satellite imagery and LIDAR results were developed using the ArcGIS Stack Profile tool. This tool averages pixel values along the geometry of the transect line.

The displacements profiles for four different transect locations measured after the Christchurch earthquake are shown as a function of distance from the river bank in Figure 10. The LIDAR displacements terminate about 30 m from the river because the LIDAR analysis could not be performed close to the river due to a lack of any topographic signature (i.e., buildings) for the LIDAR analysis. For most of the transects the remote sensing and

ground survey results are similar both in terms of the displacement distribution and maximum displacement close to the river. The agreement is particularly good for transect 1, while transect 3 shows substantially larger differences with the remote sensing results (both satellite imagery and LIDAR) showing larger displacements along the entire length of the transect. For transect 3, the measured cracks were predominately in grassy areas and many of these cracks were filled with sand, which made the measurement of their widths difficult (Martin 2014) and could explain why the ground survey displacements are smaller than those from remote sensing. Even for the best comparisons in Figure 10, there are differences as large as 0.3 m to 0.5 m between the remote sensing measurements and the ground surface measurements in some locations. The remote sensing measurements also have difficulty defining the inland extent of displacement because the displacements often do not go to zero due to the precision threshold of 0.3 m.

The displacements profiles in Figure 10 provide a detailed assessment of the remote sensing displacement results, but it is important to appreciate the differences between the ground survey measurement technique and the remote sensing measurement techniques. The ground surveys make discrete measurements of crack width, rely on precise measurements of crack width, and assume all displacements are manifested in cracks. The remote sensing measurements represent average displacements over large areas and can measure ductile movements that are not associated with ground cracking. Thus, some differences should be expected and neither technique should be considered more correct than the other. When differences are observed between the various displacement profiles, the satellite imagery results and LIDAR results tend to agree more closely with each other, indicating that the discrepancies may be due to differences in the scale of the ground survey versus the remote sensing measurements.

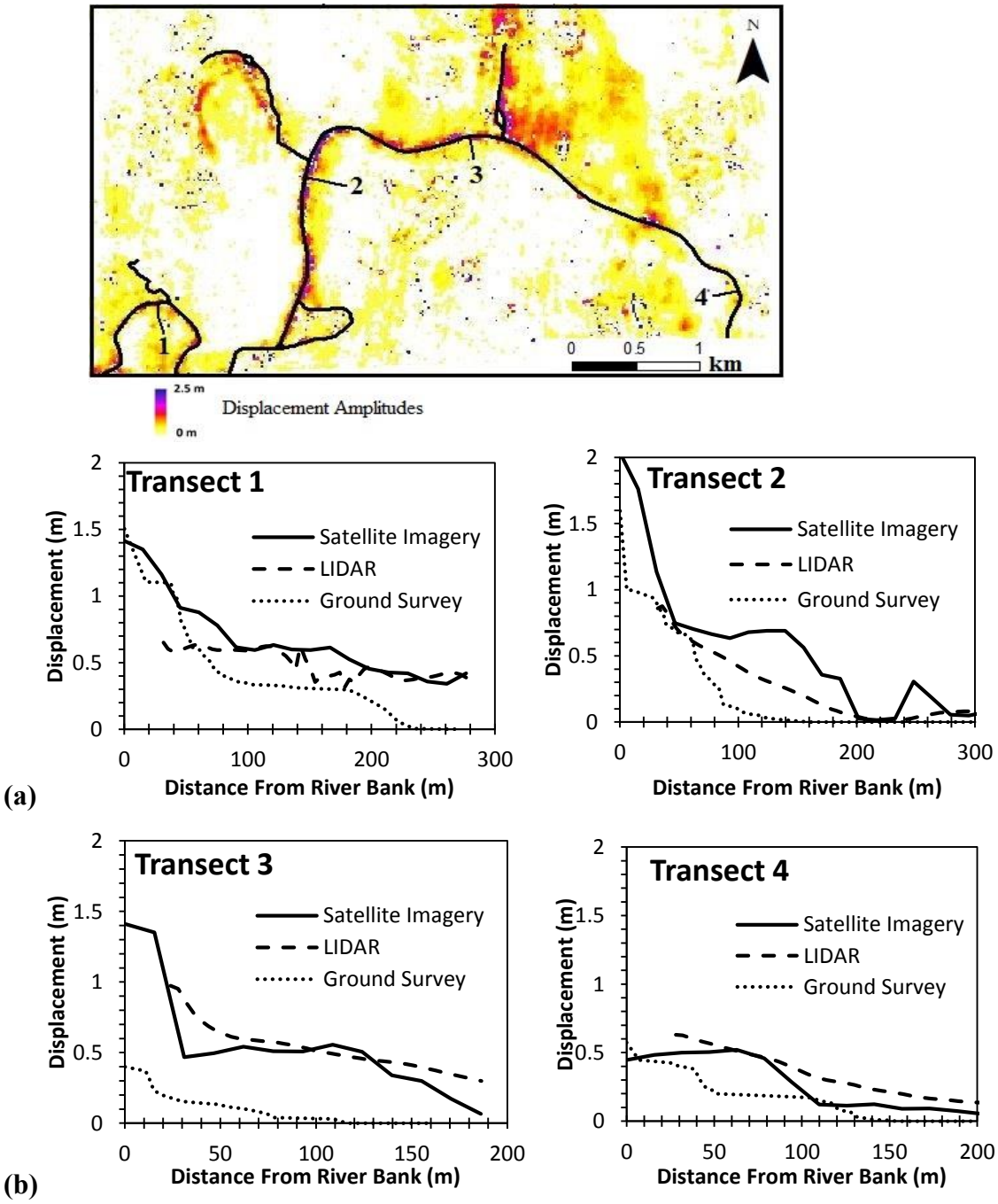

Figure 10: Comparison of lateral spreading displacements for the Christchurch earthquake computed from optical image correlation, LIDAR point cloud correlation, and inferred from field-measured crack widths along transects. (a) Transect locations and (b) displacement profiles along transects.

Appropriate image pairs with similar acquisition geometries were not identified that bracket the occurrence of 2010 Darfield earthquake, and thus lateral spread displacements could not be measured for this earthquake using optical image correlation. As an alternative, the pixel-by-pixel difference between the displacements obtained for the Christchurch earthquake and those obtained for the full Canterbury earthquake sequence was computed as a first-order estimate of the displacements that occurred during the Darfield earthquake. This approach assumes that the lateral spread displacements from the June and December 2011 earthquakes were minimal compared with the other two events, which is reasonable. The pixel-by-pixel differencing was perform using a Python script customized for this purpose.

The computed NS and EW displacements for the Darfield earthquake from the pixel differencing from the satellite analyses are compared with the corresponding displacements from correlating LIDAR displacements point clouds in Figure 11. Different areas of shown for the NS and EW displacements to better illustrate the differences. In this figure, the areas masked from the LIDAR analysis due to a lack of topographic signature are also masked from the satellite results. Note again that the LIDAR displacements show a smooth pattern due to the application of a non-local means filter. The displacement amplitudes and patterns from the pixel differencing are similar to those from the LIDAR analysis. For the NS displacements, the pixel differencing captures the displacement north of the river but the pattern of displacement is not as continuous as compared with the LIDAR displacements. For the EW displacements, the pixel differencing better captures the displacement patterns, particularly within a large portion of the oxbow lake in the northern part of the figure, as well as within the meandering river loops near the southern part of the figure.

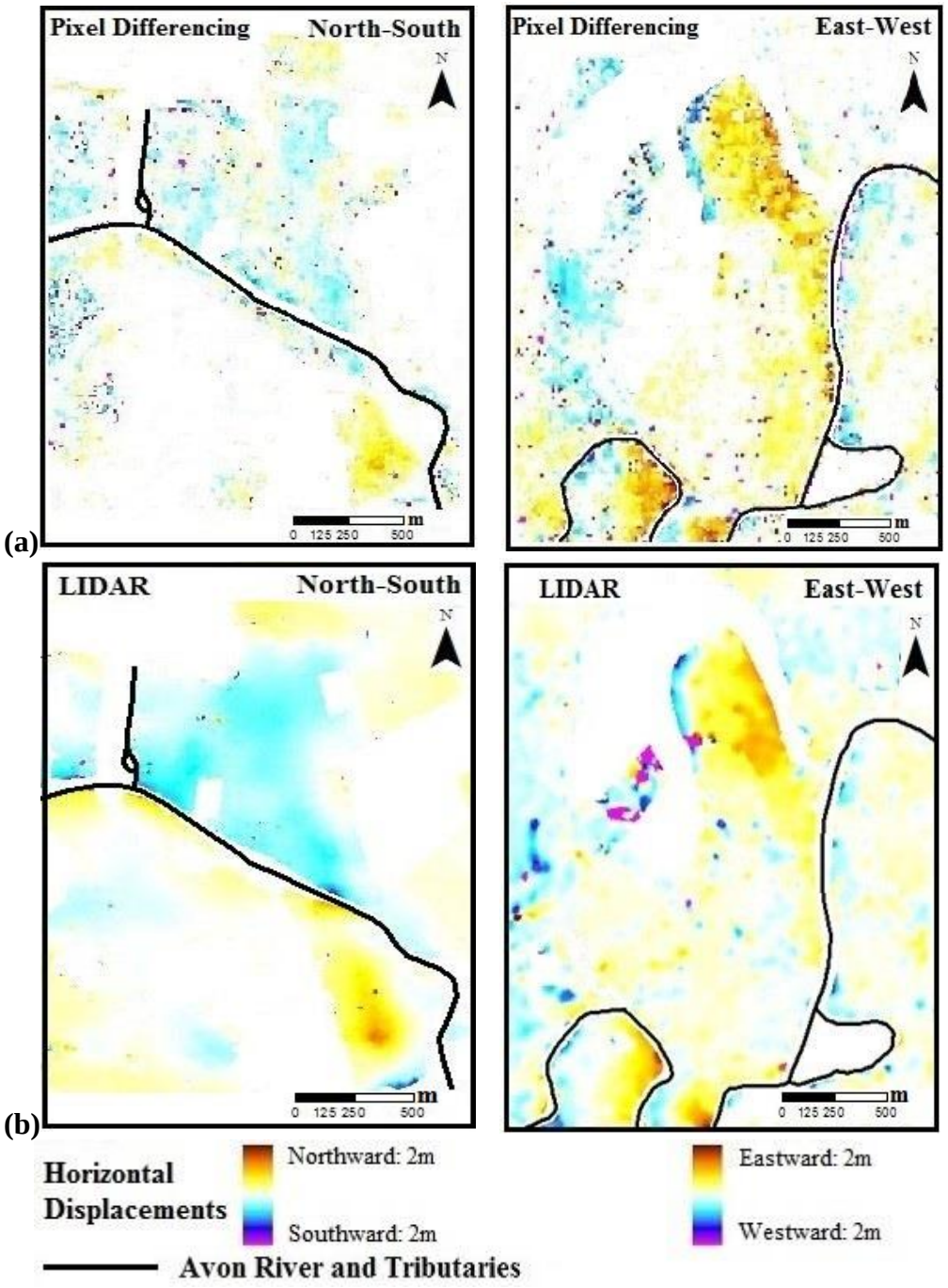

Figure 11: Horizontal displacements for the Darfield earthquake. (a) Displacements computed from pixel differencing of the satellite imagery displacements from the Canterbury earthquake sequence and Christchurch earthquake, and (b) displacements from correlation of LIDAR point clouds (Beavan et al. 2012a)

This favorable comparison indicates that such pixel differencing methods could be used to estimate displacements caused by a singular event or a multitude of events for which a specific image pair is not available, although the preference would always be to use an image pair that brackets the event of interest.

5. Conclusions

Liquefaction is a significant earthquake hazard that can generate large horizontal displacements associated with lateral spreading and these displacements cause considerable damage. To improve our understanding of liquefaction-induced lateral spreading and the models that can be used to predict the associated displacements, the collection of high quality field data on lateral spreading displacements is essential. Remote sensing techniques, in particular optical image correlation using satellite imagery, can be used for this purpose.

The quality of the displacement measurements from optical image correlation is highly dependent on the quality of the image pair used in the analysis. Using two images that have similar satellite acquisition geometries is critical. The pre-processing steps of the analysis consist of orthorectification to minimize errors due to topographic conditions and accurate alignment of the two images through co-registration. Co-registration is performed using a large set of automatically identified tie points which are common points in the two images. The final tie point set is sensitive to the parameters used by the co-registration software to identify candidate tie points. The co-registered images are used in the correlation analysis program COSI-Corr to measure displacements and these displacements are post-processed using a Python script.

Optical image correlation was applied to the Canterbury earthquake sequence, with an emphasis on the 2011 Christchurch earthquake. For both the Canterbury earthquake sequence analysis and the Christchurch earthquake analysis the precision threshold for the displacements was about 0.3 m, which means that displacements larger than 0.3 m were detectable by the method. Displacements were computed for chip windows of 64 m by 64 m, and displacement measurements were computed every 16 m.

For the Christchurch earthquake, the displacement results were compared with qualitative field observations of the severity of liquefaction and lateral spreading, as well as the general crack patterns along the Avon River. Despite the more qualitative nature of the field observations, there was a good level of agreement with the displacement measurements. The computed displacements for the full Canterbury earthquake sequence were compatible with those from the Christchurch earthquake analysis in terms of location, direction, and pattern of the displacements, but the values calculated for the Canterbury earthquake sequence were larger because they represented the cumulative displacement across multiple earthquake events. This comparison shows the consistency, repeatability, and capacity of optical imager correlation to capture the evolution of displacement across a region.

Optical image correlation analysis displacements were also compared to displacements obtained from other techniques, specifically LIDAR, air photos, and field crack measurements. The LIDAR measurements of displacement agreed well with the optical image correlation results both in terms of pattern and magnitude. The displacements derived from air photos had significant noise and although the larger displacement features could be observed, the details were masked by the noise. A more quantitative comparison was performed using displacements along four linear transects that extended perpendicular from the Avon River. The displacements along these transects had been measured in the field through the measurement of crack widths, and the cumulative crack widths along the transect were summed to produce displacement profiles that represent displacement as a function of the distance from the river. The displacement profiles from the field measurements were plotted along with the displacements from optical image correlation and from LIDAR. There was generally good agreement between the various displacement measurements, although the optical image correlation results and

LIDAR results both produced displacements somewhat larger than the field measurements. This discrepancy can be attributed to the fact that the field measurements are based on discrete measurements of crack width, while the optical image correlation and LIDAR are based on average displacements over larger areas and include displacements associated with ductile movements that may not result in cracking.

The displacements from optical image correlation for the Darfield earthquake were estimated from the pixel-by-pixel difference of the displacements from the Canterbury earthquake sequence and the displacements from the Christchurch earthquake. Although the differencing approach represents the cumulative effect of the Darfield earthquake and the other two 2011 earthquakes, the results from the differencing were still in generally good agreement with those computed from LIDAR using pre and post-earthquake LIDAR for the Darfield event. This result shows the potential of using optical image correlation to assess events that were not recorded individually, but are within a time frame for which data has been collected.

The results in this paper show that optical image correlation of satellite imagery pairs can provide accurate and detailed measurements of horizontal displacements due to liquefaction and lateral spreading. This approach can be used to create more complete and detailed databases of liquefaction-induced movements, which can be used to improve current predictive models for lateral spread displacements. Future post-earthquake investigations and research should make use of optical image correlation to document the displacements associated with liquefaction.

References

Beavan, J., Levick, S., Lee, J. and Jones, K. “Ground displacements and dilatational strains caused by the 2010-2011 Canterbury earthquakes” *GNS Science Consultancy Report* 2012/67. p. 59. (2012).

Canterbury Geotechnical Database. "Liquefaction and Lateral Spreading Observations". Map Layer CGD0300 – Christchurch earthquake (2013).

Cubrinovski M, Bradley B, Wotherspoon L, Green R, Bray J, Wood C, Pender M, Allen J, Bradshaw A, Rix G, Taylor M, Robinson K, Henderson D, Giorgini S, Ma K, Winkley A, Zupan J, O’Rourke T, DePascale G, Wells D. “Geotechnical aspects of the 22 February 2011 Christchurch earthquake.” *Bulletin of the New Zealand Society for Earthquake Engineering* 44.4 (2011): 205-226.

Debella-Gilo, Misganu, and Andreas Kääb. "Measurement of Surface Displacement and Deformation of Mass Movements Using Least Squares Matching of Repeat High Resolution Satellite and Aerial Images." *Remote Sensing* 4.1 (2012): 43-67. Print.

GDAL. 2012. GDAL - Geospatial Data Abstraction Library: Version 1.9.2, Open Source Geospatial Foundation, http://gdal.osgeo.org

Green, R., Cubrinovski, M., Allen, J., Ashford, S., Bowman, E., Bradley, B.A., Cox, B., Hutchinson, T., Kavazanjian, E., Orense, R., Pender, M., Wotherspoon, L. (2010)

Geotechnical reconnaissance of the 2010 Darfield (New Zealand) earthquake. University of Canterbury. 173pp.

Google Earth (Version 7.1.5.1557), accessed 2016.

EXELIS. "Warp and Resample." *Warp and Resample (Using ENVI) | Exelis VIS Docs Center*. N.p., n.d. Web. 23 Aug. 2013. <http://www.exelisvis.com/docs/warpingresampling.html>.

ENVI version 5.1. Exelis Visual Information Solutions, Boulder, Colorado. Used 2016.

Leprince S., S. Barbot, F. Ayoub, and J. Avouac. "Automatic and Precise Orthorectification, Coregistration, and Subpixel Correlation of Satellite Images, Application to Ground Deformation Measurements." IEEE Transactions on Geoscience and Remote Sensing 2007.

Martin, G. "Measuring Liquefaction-Induced Deformation from Optical Satellite Imagery". (2014)

Robinson, K., Cubrinovski, M., & Bradley, B. "Lateral Spreading Measurements from the 2010 Darfield and 2011 Christchurch Earthquakes". Paper presented at the Australia New Zealand Conference on Geomechanics (ANZ), Melbourne, Australia. (2012).

Robinson, K., M. Cubrinovski, P. Kailey, and R. Orense. “Field Measurements of Lateral Spreading following the 2010 Darfield Earthquake.” *Proceedings of the Ninth Pacific Conference on Earthquake Engineering* Apr. 2011: 52-60.

Scherler D., Leprince S., Manfred R. Strecker. “Glacier-surface velocities in alpine terrain from optical satellite imagery—Accuracy improvement and quality assessment”. Remote Sensing of Environment 112 (2008) 3806–3819.

USGS. Shuttle Radar Topography Mission, 3-arc second scene s44_e172_3arc_v1, Version 1.0 2004. Data available from the U.S. Geological Survey at eros.usgs.gov